Journal of Physics: Conference Series, Volume 253, Number 1, 2010, Paper Number, 012008

Computational modelling and optimisation of the fabrication of nano-structures using focused ion beam and imprint forming technologies

S Stoyanov[1], C Bailey[1], Y K Tang[1], S Marson[2], A Dyer[2], D Allen[2], M Desmulliez[3]

[1] Computational Mechanics and Reliability Group, School of Computing and Mathematical Sciences, University of Greenwich, London SE10 9LS, UK
[2] Precision Engineering Centre, Cranfield University, Bedfordshire, MK43 0AL, UK
[3] MicroSystems Engineering Centre, Heriot-Watt University, Edinburgh EH14 4AS, Scotland, UK

E-mail: s.stoyanov@gre.ac.uk

Abstract. Focused Ion Beam (FIB) and Nano-Imprint Forming (NIF) have gained recently major interest because of their potential to enable the fabrication of precision engineering parts and to deliver high resolution, low-cost and high-throughput production of fine sub-micrometre structures respectively. Using computational modelling and simulation becomes increasingly important in assessing capabilities and risks of defects with respect to product manufacturability, quality, reliability and performance, as well as controlling and optimising the process parameters. A computational model that predicts the milling depth as function of the ion beam dwell times and a number of process parameters in the case of FIB milling is investigated and experimentally validated. The focus in the NIF study is on modelling the material deformation and the filling of the pattern grooves during the mould pressing using non-linear large deformation finite element analysis with hyperelastic non-compressive material behaviour. Simulation results are used to understand the risk of imperfections in the pattern replication and to identify the optimal process parameters and their interaction.

1. Introduction

Recent demands for advanced nano- and micro-engineering have been the driving force in researching, developing and promoting the use of a number of processing technologies that have the potential for producing the required technical specifications and quality at an acceptable cost. In particular, there is a major interest and demand for the fabrication of various precision engineering parts and micro-tools, and for the production of fine small scale structures. The key issues relate to the ability to realise processes that can offer high resolution, high yield and low cost fabrication routes. These technologies are required in a wide range of applications, from the manufacturing of miniaturised components for various heterogeneous systems, to micro-fluidics, bio-medical, MEMS, and embedded test devices.

The development of nano- and micro-engineering structures, parts and components imposes a number of unique challenges [1]. Most commonly the challenges are associated with the need to use completely new, or little known manufacturing processes that may have significant uncertainty in terms of dimensional resolution and accuracy. The material behaviour at the micro-scale could also be very different to the behaviour observed in the macro-scale world. Finally, the design performance and

quality could be very uncertain as a result of the miniaturised extremely small scale nature of these products. Nowadays, the use of computational modelling and software plays an important role in studying, generating new knowledge and understanding the physical behaviour, expected quality and the risk of defects in these products, or in identifying the optimal manufacturing process control.

The computational modelling and process optimisation of two particular nano- and micro-fabrication processes, focused ion beam (FIB) and nano-imprint forming (NIF), are presented and discussed. The computational analyses focus mainly on issues related to either the optimal process control or to the risks of defects in the fabricated structures, and aim to produce results that can help to formulate design rules for improved quality, reliability and performance.

The most attractive feature of the FIB that has helped the development of this technology is its potential for direct milling and material removal while in the same time having almost no material restrictions [2,3]. In FIB milling, ion beam with certain intensity is directed to substrate material and the energised ions, when hitting the target surface, cause the transfer of the energy to the target atoms on the surface. This leads to a collision cascade and atoms from the target surface are sputtered. By moving the ion beam in a controlled manner different nano- and micro- features can be realised. The ability to control the depth variation is the most important aspect of the FIB milling process. A computational model that can be used to predict the required ion beam dwell times for a predefined shape is investigated. The emphasis is on a study for validating this model by comparing the model predictions with experimental data for milling a trench-shaped feature.

Nano-Imprint Forming process on the other side allows large scale pattering and fabrication of fine structures at very high resolution in a very cost effective manner compared with other existing processes [4]. The key concerns in this technology relate to the process control and the subsequent quality of the fabricated nano- and micro- structures. The main objective is to realise the process in a way so that the risk of defects and imperfections is minimised. In particular, a process phenomenon of significant importance for the quality of the patterns is the material deformation and the filling of the pattern grooves during the mould pressing step. We demonstrate the use of non-linear large deformation finite element analysis with hyperelastic non-compressive material behavior to study the effect of process parameters (imprint pressure and temperature) and pattern related parameters (the aspect ratio of the grooves) on the quality of the fabricated structures. The modeling results identify design rules that that can help the optimal process set up and the control of the process parameters.

2. Computational Modelling of FIB

The principle of operation for FIB is bombardment of a target surface through high energy gallium Ga^+ (or other) ions. As a result of this, small amount of material sputters in the form of secondary ions, natural atoms and secondary electrons. The ion beam is moved in a raster scan manner which is digitally controlled over a pixel matrix defined on the target surface area. The size of a pixel is determined by the step of the beam movement. The time the ion beam spends on a pixel is called dwell time. The sputtering yield is the measure for the efficiency of the material removal and depends on a number of parameters such as the ion energy, angle of incidence of the ions to the target surface, ion flux and mass of the ions and target material atoms.

2.1. Computational Model for FIB sputtering

The first models for simulation of ion beam milling have been limited in the sense that they tried to provide predictions for the final geometry based on a particular set of FIB parameters. The requirements for the FIB process at present are much more demanding than its original ion milling abilities. In particular, a critical control required for FIB milling is the one of the depth variation.

A mathematical model that can be used to predict the etched shape or to calculate the dwell times required to achieve a predefined shape is investigated [5]. The model relates the milling depth and the ion beam dwell times at the pixels placed over the target surface using a number of process parameters. The governing equation for the sputtering process is then discredited over each element of

the pixel matrix so that ultimately a system of linear equations that relates the dwell times t_{ij} with the sputtering depth H_{ij} at any pixel (i,j) is constructed.

If (x_i, y_j) denotes the centre of the pixel (i,j), then the sputtering at this pixel in terms of depth as a result of the material removal at that pixel can be expressed as

$$H_{ij} = \iint \frac{\Phi(x,y)}{\eta} \; f_{x,y}(x_i, y_j)\, Y(E_0, \alpha_{x_i,y_j})\, t_{x,y} \; dxdy \tag{1}$$

where H_{ij} is the sputtering depth at the point (x_i, y_j), $\Phi(x,y)$ is the ion flux at point (x,y) on the target surface ($cm^{-2}s^{-2}$), η is the atomic density of the target material (atoms/cm^3), $Y(E_0, \alpha_{x_i,y_j})$ is the sputtering yield (atoms per incident ion at point (x_i, y_j)), $t_{x,y}$ is the dwell time of the ion beam at point (x_i, y_j) (seconds), $f_{x,y}(x_i, y_j)$ is the ion beam density distribution function in two dimensions.

The sputtering yield in Equation (1) is function of the angle of incidence α_{x_i,y_j} of the ion beam at point (x_i, y_j) and the ion energy E_0 as well as the type of ion source and target material. Generally, the yield increases from perpendicular ion beam incidence to a maximum at angle 60° to 85°, and then rapidly decreases due to the strong reflection at grazing incidence. The sputtering yield can be obtained experimentally. A software package, SRIM (The Stopping and Range of Ions in Matter), can be also used to predict the sputtering rate for particular ion source and target material under specified energy conditions by Monte Carlo binary collision simulation [6].

In FIB milling, the ion flux is not uniform and has a distribution associated with it. Typically, it is assumed that this distribution is Gaussian. The standard deviation of the distribution can be estimated by assuming that the beam spot diameter is equal to full width at half maximum (FWHM). The ion beam geometry in terms of density distribution $f_{x,y}(x_i, y_j)$, as required in the FIB model above, is taken to be Gaussian bi-variate density function:

$$f_{x,y}(x_i, y_j) = \left(\frac{1}{\sqrt{2\pi}\sigma} \right)^2 e^{-r^2/(2\sigma^2)} \tag{2}$$

where $r^2 = (x_i - x)^2 + (y_j - y)^2$ is the radial coordinate for an ion beam focused at (x,y).

2.2. FIB Experiment and Model Validation

Two FIB experiments using FEI 200 FIB machine with gallium ion source and silicon wafer as the target surface are conducted. The results from the first experiment are intended to provide data on the actual sputtering yield, and the second test is undertaken to examine the predictive capability of the model and for model validation.

2.2.1. *Experimental derivation of the sputtering yield*

The FEI FIB 200 system is used to set the milling of a simple boxed shaped feature. The objective is to estimate the amount of sputtered material and knowing the process parameters to obtain experimentally a value for the sputtering yield for the particular set of FIB process conditions. The target material used in the study is p-Silicon (B doped)-(100) orientation, and the scanned area on the target surface is selected with dimensions 5x10 μm. The ion beam is set with current 350 pA (corresponding to beam diameter 55 nm). The beam is set to raster with 50% overlap, angle of incidence 0 degrees (perpendicular to the target surface), ion energy 30 keV and at dwell times of 1 μs. The FIB current of 350 pA with overlap 50% is associated with ion flux of 1.44e24 ions/sec m^2 at the target surface. The total time of milling for this experiment is set to 460 sec this resulting in 13,890 beam scans over the target area.

The cross sectional analysis shows some variation in the depth of the produced shape ranging from 0.883 μm to 1.09 μm (Fig. 1). From the analysis profiles we calculate that the sputtered volume is 48.176 μm^3. For total time of milling equal to 460 sec and ion beam current of 350 pA, the total amount of ions delivered to the sample over this milling period of time is 1.00488e12 ions. With known atomic density of the target material (5e10 atoms/μm^3), we can now evaluate the average sputtering yield. The calculated sputtering yield value is 2.397 atoms/ion. This experimentally derived value is well in the range that can be found in the literature and very similar to the SRIM software prediction.

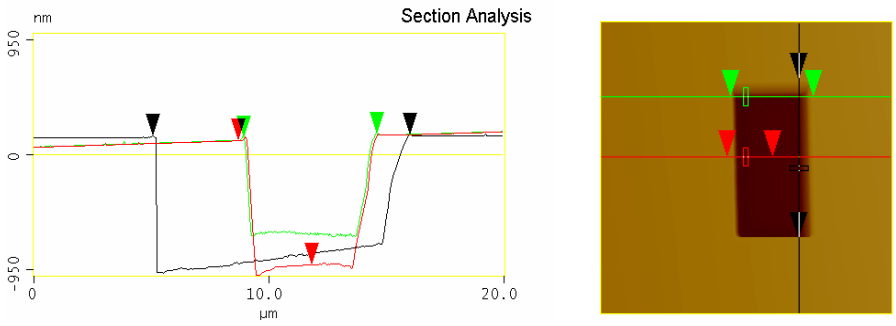

Figure 1. Cross sectional analysis of the milled shape (sputtering yield case study).

2.2.2. *Model Validation*

The validation example is designed with experiment of milling a step-wise parabolic trench using the same FIB system (FEI 200) and the same FIB process settings as used in the previous study. The desired trench has depth at the centre line 1.94 μm. The target area on the silicon surface that defines the trench is 10 x 10 μm.

The parabolic step-wise cross-section of the targeted shape for the trench, as shown in Figure 2, features five patterns. The top most (at the surface) is pattern 1, the bottom most is pattern 5. The width of each subsequent pattern is reduced by 2 μm of the width of the pattern above. The width of pattern 1 is 10 μm. Note that in Figure 2 the horizontal and the vertical axis are not equally scaled. The depth at each of the five patterns that realise the shape of interest are detailed in Table 1.

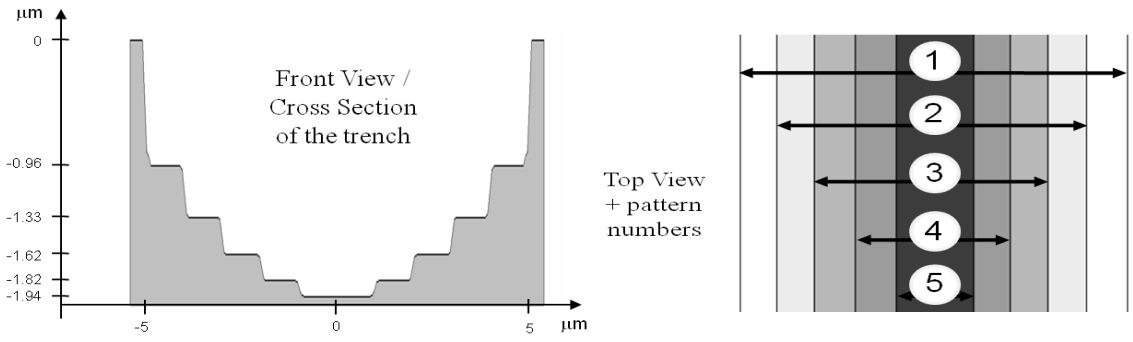

Figure 2. Shape dimension of the trench feature used in model validation study

Table 1. Definition of the parabolic shape depth variation.

Pattern n	**1**	**2**	**3**	**4**	**5**
Set depth values from FIB model (μm)	0.96	1.33	1.62	1.81	1.94

The computational model discussed in the previous section is employed to make predictions for the required pixel dwell times to mill this predefined shape. The model parameters are detailed in Table 2 and based on process milling as used in the experiment for verifying the sputtering yield values.

Table 2. FIB model parameters.

Parameter	Value
Target material atomic density	5 x 10^{22} atoms/cm^3
Beam Spot diameter	55 nm (Full Width at Half Maximum, FWHM)
Ion beam flux	1.446e12 ions / mm^2 sec
Beam overlapping	50% (pixel size : dx = 55 nm, dy = 27.5 nm)
Ion beam distribution	Gaussian bi-normal, with standard deviation 0.02786 μm
Sputtering rate	2.39 atoms/ion (experimentally derived)

The computational model for FIB is discretised over the pixel matrix with individual pixel dimension 55 x 27.5 nm. The required depth at each pixel is specified so that the sputtered shape corresponds to the five pattern step-wise shaped trench targeted with this experiment. The system of equations is solved for the unknown dwell times. The solution is detailed in the first two columns of Table 3. The modelling results indicate the dwell times if the entire shape is milled in a single scan.

In order to apply the modelling predictions for the dwell times to a real experiment with the FEI 200 system, the model outputs must be transformed into an appropriate input data for the machine. In particular, the milling of such a shape would always be attempted not in a single beam scan but ratter using a large number of scans. For a feature with variable depth such as the five level step-wise trench considered in this study, the FIB system can be set in one of the following two regimes. First option is to execute a fixed number of iterations across all pixels using different pixel dwell times to achieve the shape. Alternatively, the FIB can be run into mode where the dwell time is fixed for all pixels but different pixels are scanned different number of times (so called pattern mode). Both settings are equivalent as there is a linear direct relationship between the pixel dwell time and the number of scans at that pixel. Because the FEI 200 can be set with fixed dwell time for all pixels and allows to define patterns that will be subjected to different number of scans. The model predictions are transformed into an equivalent FIB set up in terms of number of scans on each pattern, respectively into total time for scanning each particular pattern. The data is shown in the last two columns of Table 3.

Table 3. FIB model predictions for dwell times and the eequivalent FEI FIB 200 set up.

Pattern number	Model predictions for pixel dwell time, final shape in one scan	Equivalent FEI FIB 200 set up (fixed dwell time 1 μs and different pattern scanning times, respectively number of scans	
	Dwell time (μs)	Number of beam scans over the respective pattern	Total (cumulative) time for scanning the pattern area (sec)
1	13,706	13,706	908
2	19,257	19,257	1,203
3	23,403	23,403	1,369
4	26,227	26,227	1,443
5	27,905	27,905	1,465

The milling of the trench is undertaken in five steps that correspond to milling each pattern area, in a sequence, for the identified respective total time for that pattern. Pixel dwell time is predefined at 1 μs. Because the last column in Table 3 specifies the cumulative time for milling the respective pattern area, in reality the total scanning time at any pattern is the incremental time from the previous milling time. For example, we start with milling the area of pattern 1 for time 908 sec, then we continue with milling the area which corresponds to pattern 2 for time 295 sec (the increment from pattern 1), etc.

Figure 3 shows the output data and graphs form a cross sectional analysis undertaken to obtain information for the actual shape and the trench depth variation. Several cross sectional planes are examined. Table 4 details the depths as defined and used in the model, the actual measured depths for the experimentally sputtered shape, and also provides the percentage errors between the two values.

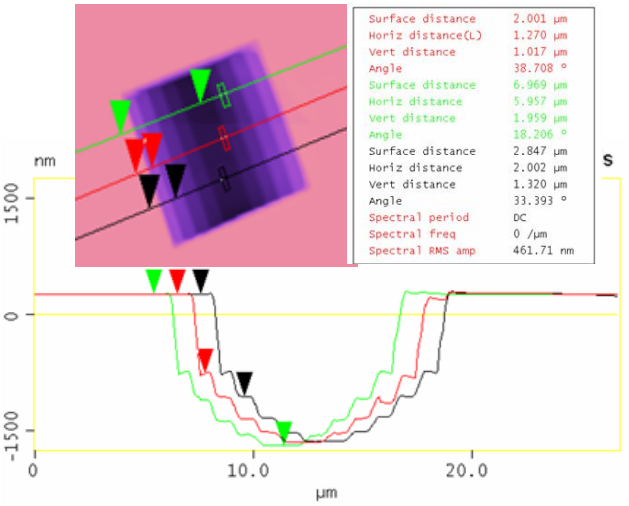

Figure 3. Cross sectional analysis of the sputtered trench (model validation case study).

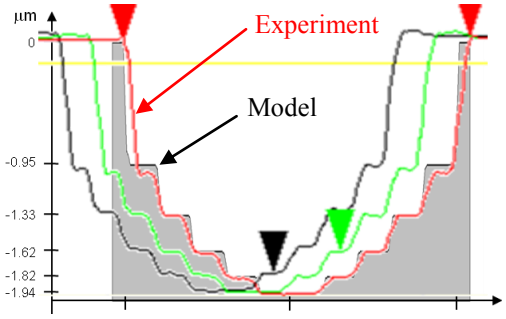

Figure 4. Model vs. experimental cross-sectional profiles.

Table 4. Comparison between model and experimental data for depth variation.

Pattern number	1	2	3	4	5
Set Z values from FIB model (mm)	0.96	1.33	1.62	1.81	1.94
Z measured (μm) ± 0.03 from sectional analysis	1.01	1.32	1.61	1.80	1.96
Difference in model and experimental cross-sectional depths (%)	5.0	0.8	0.6	0.5	1.0

The data in Table 4 shows that there is a very good agreement between the intended shape as analysed with the model and the actual experiment set with the model predictions (see also Fig. 4). Only at the level of the first top most step the difference in depth between the model and the experiment is larger at 5 %. The depth at all other subsequent patterns is extremely well predicted, with errors less than one percent. At the centre line of the trench the model predictions is for depth 1.94 μm versus the experimental measurement of 1.96 μm. The model validation study has shown that the FIB computational model can be used as a powerful tool to predict how to set the FIB system in order to accurately achieve the desired shape without following a trial-and-error approach. However, it is critical to use accurate model input data related to the process parameters, in particular the sputtering yield and also to account for variation in the FIB process parameters.

3. Computational Modelling and Simulation of Nano-Imprint Forming

The principle of the generic NIF process involves several steps: (A) softening (above Tg) of a thin film of formable material deposited on a substrate, (B) pressing a rigid mould which has the required

(negative) pattern of features onto the formable material, (C) curing the formable material by cooling down to temperatures below Tg, and finally (D) releasing the mould. The sequence of these process steps results in a negative replication of the mould pattern onto the formable material with process ability for very high resolution [7]. Figure 5 outlines schematically the imprint forming process steps.

Whereas conventional techniques use convection heating, the NIF approach considered in this paper uses focused microwave radiation to soften the material. This method has already been investigated for a different application by using advanced multi-physics modelling techniques to simulate the physical phenomena and process issues related to microwave heating [8, 9]. The focus in this work is on modelling the mould pressing step only (step B in Figure 5).

3.1. NIF Mould Pressing Step - Modelling and Simulation Results

Most applications in NIF are based on polymeric materials that have suitable properties for the particular method of softening the material. In this investigation Poly-Methyl MethaAcrylate (PMMA) with glass transition temperature (Tg) 105°C is studied. Above Tg, the target PMMA material is soft and the pressing of the mould into the polymer promotes the flow of the formable material into the mould pattern grooves. The actual elevated temperature to which the polymer is taken and then deformed is an important process parameter. The imprint temperature is not an independent process parameter. For example, higher imprint temperature is associated with lower imprint pressure at the expense of longer process steps.

The imprint pressure is another process parameter that has a major impact on the quality of the replication. An insufficient pressure will result in incomplete filling of the pattern grooves and may lead subsequently to shape defects. Conversely high imprint pressures should also be avoided as this will cause high residual stresses in the cured polymer during the subsequent process steps. Therefore one of the most important parameters to be optimised is the imprint pressure.

The deformation process and the process parameters are also influenced by the shape of the pattern and the aspect ratio (AR) of the grooves. Important relationships between the process parameters are identified and design rules for accurate and defect-free replications are formulated using the modelling results. In this work the effects of the step dwell times are not analysed.

3.1.1. Computational Model

Above Tg the PMMA is assumed do behave as non-compressive rubber-like hyper-elastic body. The Money-Rivlin hyper-elastic model is used to model the large deformations during the deformation process. The constants at different temperatures required by the Money-Rivlin material model used to simulate the visco-elastic behavior of the PMMA above Tg are discussed and reported in reference [10]. In all simulations that follow the mould is modelled as a rigid body. The analysis is also set as a large strain and large deformation analysis. Finally, contact boundary and interfaces between the mould and the polymer are included. No friction is assumed between the mould and the polymer. The simulations are carried out using ANSYS software. Hirai et al. have validated through experiments the above modelling approach in the simulation of the dynamics of the deformation process for thermal nanoimprint lithography [11].

The finite element analysis model of the pressing step is two-dimensional and comprises a single groove section of the mould pattern and the associated part of the formable material. A nominal case is designed to simulate the deformation process at imprint temperature of 170^{o}C and for mould pattern where the groove has height and width of 300 nm resulting in aspect ratio AR=1. The thickness of the PMMA is also 300 nm. The nominal model is illustrated in Figure 6.

3.1.1. Effect of Imprint Pressure

To understand the effect of imprint pressure, the nominal case is run with several different pressures and the deformation profile is observed. This parametric study is used to understand what percentage of the groove is filled as a result of applying various in value imprint pressures P and ultimately to indicate the nominal pressure P_0 required. The nominal pressure P_0 is the pressure at which the groove

is completely filled with material. We also define a quantity called relative imprint pressure, P_R. The relative imprint pressure is the ratio of the applied pressure and the nominal pressure, $P_R=P/P_0$, and provides a more generic interpretation of the simulation results in terms of relative quantities. Figure 7 shows the simulated polymer deformation profile at four different relative imprint pressures and details the percentage, in volume, of the groove which is successfully filled. This quantity is defined as the filling ratio. The relationship between the relative imprint pressure and the filling ratio is non-linear. For example, at 1/3 of the nominal imprint pressure, about half of the groove is penetrated by the polymer and at imprint pressure of half the nominal pressure about 76% of the groove is successfully filled. The existing trend is illustrated in Figure 8.

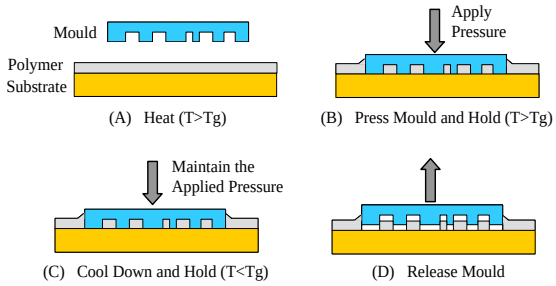

Figure 5. Schematic outline of imprint forming generic process steps.

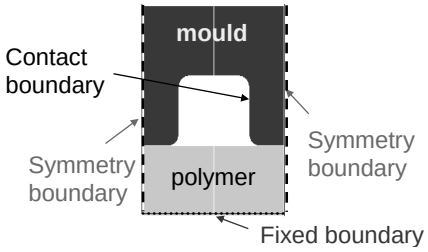

Figure 6. Imprint forming model and boundary conditions.

The simulation results of the nominal case show that the absolute value of the required nominal pressure P_0 that can promote a complete filling of the pattern is 2.28 MPa. It is useful to consider the nominal imprint pressure in relation with the polymer elastic modulus, E_0, at the relevant imprint temperature. The required nominal imprint pressure P_0 for the nominal case at imprint temperature 170°C is approximately twice the elastic modulus, $P_0=1.9E_0$. The ratio P_0/E_0 defines the normalised imprint pressure P_N that can be used as a relative process parameter to indicate the imprint pressure relations to the formable material behavior and properties.

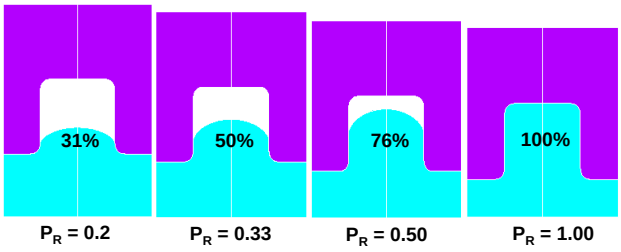

Figure 7. Deformation profiles from simulations at different relative imprint pressures vs. filling ratio.

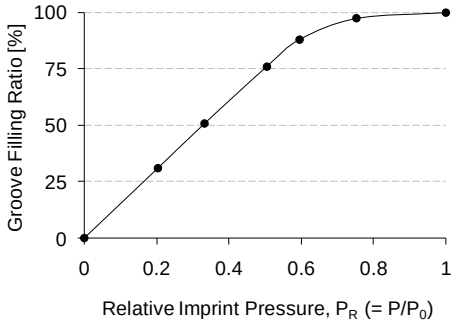

Figure 8. Relative imprint pressure vs. filling ratio.

3.1.2. Effect of the Aspect Ratio of the Grooves in the Pattern

The pattern aspect ratio (AR) is defined as the ratio of groove height over groove width. In order to fill in completely patterns with different aspect ratios, different nominal imprint pressures are required. To gain knowledge on the pressure trends, three different aspect ratio cases (0.5, 1, and 1.5) are modelled and analysed as illustrated in Figure 9.

The different aspect ratios are achieved by varying the width of the grooves and by keeping the height constant at 300 nm as in the nominal case. The thickness of the PMMA layer is also unchanged at 300 nm. The three aspect ratio cases are simulated at 170°C.

The results show that, for higher aspect ratio, higher imprint pressure is required to achieve a complete filling of the pattern. Figure 10 illustrates the simulated data in terms of aspect ratio vs. normalised imprint pressure P_N. Simulation results indicate non-linear relationship between AR and the imprint pressure. With exactly the same process conditions and materials as used for the analysis of the nominal case, increasing only the pattern aspect ratio from 0.5 to 1.5 would require 45% higher imprint pressure to ensure accurate shape replication.

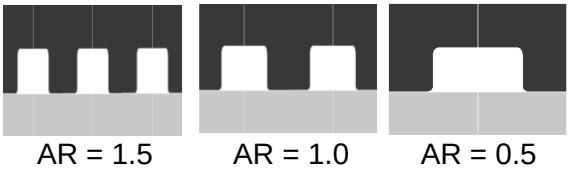

Figure 9. Aspect ratio cases.

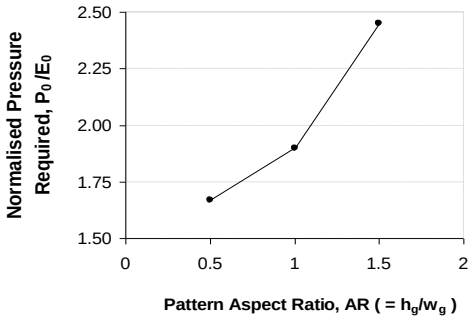

Figure 10. Aspect ratio vs. imprint pressure.

3.1.3. Effect of Imprint Temperature

The PMMA shows different material behavior at different imprint temperatures because the viscous flow properties change. Therefore, the imprint temperature as a process parameter has influence on the other process parameters. The aim of this part of the study is to evaluate the requirements for imprint pressure when the imprint forming is undertaken at different temperatures. To model this effect, the data for PMMA visco-elastic behaviour at temperatures 150, 170 and 190°C is used [10]. The simulations undertaken to evaluate the relationship between the imprint temperature and the imprint pressure are based on the nominal case pattern scenario.

As expected, because at higher temperatures the polymer becomes less viscous and easy to deform, lower imprint pressure need to be applied. As Figure 11 shows, the required imprint pressure lowers when the imprint temperature increases. For the PMMA investigated in this work and in terms of absolute values, it is predicted that the imprint pressure at temperature 150°C is 3.3 MPa and at temperature 190°C the imprint pressure is over two times lower (1.4 MPa).

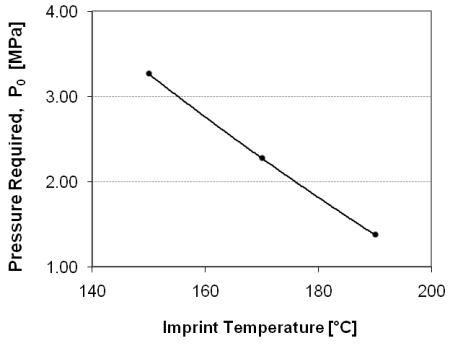

Figure 11. Imprint temperature vs. imprint pressure.

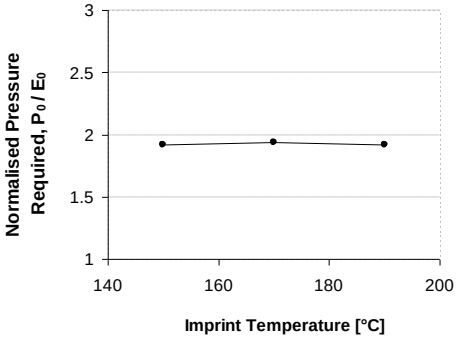

Figure 12. Imprint temperature vs. normalised imprint pressure.

The relationship between the imprint temperature and the normalised imprint pressure P_N ($=P_0/E_0$) provides further insight into the existing trends. Elastic modulus E_0, here, is different at different temperatures. The graph in Figure 12 reveals an interesting result. The normalised imprint pressure is virtually independent of the imprint temperature and, for the nominal case of the pattern geometry and the PMMA being analysed, it is close to constant 1.9.

4. Conclusions

Computational approach to study two nano- and micro-manufacturing processes, FIB and NIF, is researched and presented. A computational model for estimating FIB milling dwell times to achieve predefined shapes is validated. The analysis has shown that the model accuracy is very good. In the case study reported the difference in the depth of a parabolic step-wise trench predicted with the model and observed in the experiment was 1%. Clearly, variations do exists in the process and there is also some uncertainty associated with the process parameters. Quantifying the effect of these uncertainties and incorporating their effect in the model as part of a risk analysis assessment is where we focus our interest at present. Additional computations that account for re-deposition effects are also considered though more relevant in scenarios of milling high aspect ratio features.

The simulation results on the NIF process have provided insights into the potential risks associated with the technology and have shown trends that can help minimising commonly observed defects. For the particular PMMA polymer studied in this work the optimal imprint pressure was identified. The imprint pressure is the most important parameter that can result in shape imperfections if not optimised. This parameter depends also on other process parameters such as the imprint temperature and the aspect ratio of the grooves. Future work will address the effect of other process parameters such as the dwell times of the process steps and issues that are specific to the way in which the formable material is soften. An effort will be placed also on gathering relevant material and process data required by simulation models.

Acknowledgments
The authors acknowledge the UK funding council - ESPRC - for supporting the work detailed in this paper and in particular the 3D-MINTEGRATION project under grant EP/C534212/1.

References

[1] Desmulliez M and Topham D 2008 3D-Mintegration: the design and manufacture of 3D miniaturised integrated products, *Proc. 2nd ESTC*, London, 737-41
[2] Gamo K 1993 Focused Ion Beam technology, *Semicond. Sci. Technol.* **8** 1118-23
[3] Tseng A A 2004 Topical review: recent developments in micromilling using ion beam technology, *J. micromechanics and microengineering*, **14** 15-34
[4] Chou S Y and Krauss P R 1997 Imprint lithography with sub-10 nm feature size and high throughput, *Microelectronics Engineering* **35** 237-40
[5] Nassar R, Vasile M, Zhang W, 1998 Mathematical modelling of focused ion beam microfabrication, *J. Vac. Sci. Technol. B* **16** (**1**) 109-15
[6] SRIM2010, http://www.srim.org/
[7] Chou S Y, Krauss P, 1997 Imprint Lithography with sub-10 nm Feature Size and High Throughput, *Microelectronics Engineering* **35** 237-40
[8] Tilford T, Sinclair K, Bailey C, Desmulliez M, Goussettis G, Parrott A and Sangster A 2007 Multiphysics Simulation of Microwave Curing in Micro-Electronics Packaging Applications, *Journal of Soldering and Surface Mount Technology* **19** (**3**) 26-33
[9] Sinclair K, Desmulliez M and Sangster A 2006 A Novel RF-Curing Technology for Microelectronics and Optoelectronics Packaging, *Proc 1st Electronics System-Integration Technology Conference* 1149-57
[10] Stoyanov S, Amalou F, Sinclair K, Bailey C and Desmulliez M 2008 Modelling the nano-imprint forming process for the production of miniaturised 3D structures, *Proc 9th EuroSIME* 497-504
[11] Hirai Y, Fujiwara M, Okuno T, and Tanaka Y 2001 Study of the resist deformation in nanoimprint lithography, *J. Vac. Sci. Technol. B* **19** (6) 2811-15